

PROPER MOTIONS OF PSRS B1757–24 AND B1951+32: IMPLICATIONS FOR AGES AND ASSOCIATIONS

B. R. ZEIGER¹, W. F. BRISKEN², S. CHATTERJEE^{3,4}, W. M. GOSS²

ApJ, accepted

ABSTRACT

Over the last decade, considerable effort has been made to measure the proper motions of the pulsars B1757–24 and B1951+32 in order to establish or refute associations with nearby supernova remnants and to understand better the complicated geometries of their surrounding nebulae. We present proper motion measurements of both pulsars with the Very Large Array, increasing the time baselines of the measurements from 3.9 yr to 6.5 yr and from 12.0 yr to 14.5 yr, respectively, compared to previous observations. We confirm the nondetection of proper motion of PSR B1757–24, and our measurement of $(\mu_\alpha, \mu_\delta) = (-11 \pm 9, -1 \pm 15)$ mas yr⁻¹ confirms that the association of PSR B1757–24 with SNR G5.4–1.2 is unlikely for the pulsar characteristic age of 15.5 kyr, although an association cannot be excluded for a significantly larger age. For PSR B1951+32, we measure a proper motion of $(\mu_\alpha, \mu_\delta) = (-28.8 \pm 0.9, -14.7 \pm 0.9)$ mas yr⁻¹, reducing the uncertainty in the proper motion by a factor of 2 compared to previous results. After correcting to the local standard of rest, the proper motion indicates a kinetic age of ~ 51 kyr for the pulsar, assuming it was born near the geometric center of the supernova remnant. The radio-bright arc of emission along the pulsar proper motion vector shows time-variable structure, but moves with the pulsar at an approximately constant separation $\sim 2.5''$, lending weight to its interpretation as a shock structure driven by the pulsar.

Subject headings: pulsars: individual (PSR B1757–24, PSR B1951+32) — ISM: individual (G5.4–1.2, CTB 80) — stars: neutron — supernova remnants

1. INTRODUCTION

Neutron stars (NSs) are born from the core collapse of massive stars, whose deaths are marked by supernova remnants (SNRs). Measuring the proper motions of young NSs allows their trajectories to be traced back, and can thus provide strong tests of proposed NS-SNR associations. In cases where such associations can be confirmed, an independent age estimate can be derived for both the NS and its associated SNR.

However, such an exercise is subject to several pitfalls. On one hand, a typical radio pulsar might be detectable for $\gtrsim 10^7$ yr, while the associated SNR fades into the interstellar medium (ISM) in $\lesssim 10^5$ yr, leaving behind young pulsars with no detectable SNRs. On the other hand, there are also several SNRs with no associated pulsars. Not all NSs are radio pulsars, but when young, they are all likely to be bright in thermal X-ray emission, as illustrated, for example, by the detection of point sources in the SNRs Kes 73 (Vasisht & Gotthelf 1997) and Kes 79 (Seward et al. 2003). The absence of such X-ray detections in a set of nearby, young SNRs (Kaplan et al. 2004, 2006) aggravates the problem. While unusual cooling scenarios may be required for NSs in these young SNRs, a partial explanation for the “missing” NSs might lie in their birth velocities. Radio pulsars have characteristic birth velocities ~ 400 – 500 km s⁻¹ (Arzoumanian et al. 2002; Hobbs et al. 2005), and they are likely to escape

their natal remnants once the expansion of the SNR is decelerated by the ISM, making identification of pulsar-SNR pairs problematic.

Thus, cases where a young radio pulsar can be associated with a SNR are particularly important. The pulsars B1757–24 and B1951+32 present two such situations in which associations might be possible. Both are young pulsars with high spin-down energy-loss rates, and in both cases, the ram pressure balance between the NS relativistic wind and the ISM produces a pulsar wind nebula (PWN) with a bow shock structure. PSR B1757–24 appears to be exiting the approximately circular SNR G5.4–1.2, whose asymmetric brightness, in conjunction with the PWN produced by the pulsar, produces the structure known as “the Duck” (see Fig. 1). Meanwhile, PSR B1951+32 drives a complex interaction within the SNR CTB 80 (G69.0+2.7; see Fig. 2), including a radio-bright structure resembling a bow shock in the direction of its motion.

We present Very Large Array (VLA) observations that improve the time baseline for the proper motion measurements of these two pulsars. In §2 we detail the observations, analysis, and results for PSR B1757–24, and likewise for PSR B1951+32 in §3. We discuss the implications of our results in §4.

2. PSR B1757–24: OBSERVATIONS AND RESULTS

PSR B1757–24 is an energetic young pulsar, with a period $P = 125$ ms, a spindown energy loss rate $\dot{E} = 10^{36.4}$ erg s⁻¹, and a characteristic age $\tau_c \equiv P/2\dot{P} = 15.5$ kyr. As shown in Figure 1, its location and the morphology of its PWN suggest that it is escaping the circular SNR G5.4–1.2 (Frail & Kulkarni 1991; Manchester et al. 1991). If it was born at the center of

¹ Center for Astrophysics and Space Astronomy, University of Colorado, Boulder, CO 80304; zeigerb@colorado.edu

² National Radio Astronomy Observatory, Socorro, NM 87801; wbrisken, mgoss@aoc.nrao.edu

³ School of Physics, The University of Sydney, NSW 2006, Australia; schatterjee@usyd.edu.au

⁴ Jansky Fellow

the remnant and its characteristic age is close to its real age, that would imply a proper motion $\sim 70 \text{ mas yr}^{-1}$ and a transverse velocity $\sim 1500\text{--}2000 \text{ km s}^{-1}$, high compared to the radio pulsar population. However, Gaensler & Frail (2000) placed an upper limit on the motion of the PWN that was inconsistent with such a high velocity, and suggested that the true age of the pulsar was much larger than the characteristic age. Thorsett et al. (2002) derived comparable limits on the proper motion⁵ of the pulsar (rather than the PWN) of $(\mu_\alpha, \mu_\delta) = (-2.1 \pm 7.0, -14 \pm 13) \text{ mas yr}^{-1}$ and suggested instead that the proximity of B1757–24 and G5.4–1.2 was merely a line-of-sight coincidence in the crowded region near the Galactic center. Arguments for and against an association between the pulsar and SNR were summarized by Blazek et al. (2006), who improved the upper limit on the westward proper motion of the PWN and concluded that both interpretations for the Duck (a line-of-sight coincidence and a genuine association with a large age) remained viable.

Based on the dispersion measure, PSR B1757–24 is estimated to lie at a distance of $5.2 \pm 0.5 \text{ kpc}$ (Cordes & Lazio 2002), while the distance to G5.27–1.2 is greater than 4.3 kpc based on H I absorption (Frail et al. 1994; Thorsett et al. 2002). Here we adopt a distance of $5d_5 \text{ kpc}$.

2.1. Observations

VLA observations of PSR B1757–24 spanned 6.4 yr, from 1998 to 2004. The 1998 June 03 epoch was observed using the BnA configuration; all of the later epochs used the A configuration. At the frequency of observation, 1.45 GHz, the A configuration resolution at a declination of -25° is $\sim 1.2'' \times 2.2''$, elongated north-south. The first three epochs employed the pulsar gate on the right circular polarization to allow increased sensitivity in the pulsar measurements by only accepting data when the pulsar was “on.” The 2002 February 21, 2002 May 02, and 2004 December 09 epochs included the Pie Town VLBA antenna, more than doubling the maximum east-west baseline length. The ungated data from the 2002 February 21 epoch was not used, as the observation was not long enough to provide sufficient u - v coverage and sensitivity needed for clear identification of the pulsar. In order to minimize variation in u - v coverage between epochs and in contrast to Thorsett et al. (2002), we do not use the Pie Town baselines. Observations were made in the ‘2AD’ correlator mode, offering 15 spectral channels each of width 1.56 MHz in both circular polarizations and allowing a usable field of view of $\sim 30'$. Details of these observations are shown in Table 1.

The data were calibrated using standard procedures within the AIPS⁶ package. Sources 3C 286 and 3C 48 were used as flux density and bandpass calibrators and 1751–253 was used for phase calibration. The AIPS task UVFIX was used to recalculate the UVW coordinates incorporating aberration corrections not performed by the VLA online system. Given the large field of view and the sparse distribution of sources with compact structure, we selected 14 sub-regions of the field (containing the pulsar

and 13 other apparently compact sources) for imaging. These fields were jointly deconvolved to produce initial images. Two self-calibration and imaging iterations were performed using all 14 sub-regions to generate the final images used for the astrometry.

Positions of reference sources and the pulsar were determined with a Gaussian fit using the AIPS task JMFIT. The proper motion of the pulsar was measured with respect to a reference frame defined by six point sources chosen based on compactness from the 13 imaged sub-regions. The reference source positions and fluxes from the (ungated) 2004 December 09 epoch are listed in Table 2, and our method is described in greater detail in McGary et al. (2001).

The $10''$ PWN in which the pulsar is embedded is resolved out by our observations, but it contributes an additional uncertainty to the position of the pulsar in the ungated data. To account for the $\sim 50\%$ increase in rms noise within this region relative to the background, the pulsar position uncertainties were increased in ungated epochs by a factor of 1.5. In the gated data, the PWN contribution to the noise is insignificant and the position uncertainties of the reference sources dominate the proper motion uncertainty.

2.2. Results

The structure of the PWN around the pulsar is uncertain and could cause a systematic offset in the measurement of the pulsar position, affecting registration between the gated and ungated data sets. Thus, we measure the proper motion of the pulsar separately for the gated and ungated data and combine the two independent results for a final proper motion value. Using ungated data, we measure a proper motion of $(\mu_\alpha, \mu_\delta) = (-16.9 \pm 12.6, -35.8 \pm 22.4) \text{ mas yr}^{-1}$; with gated data, we measure $(\mu_\alpha, \mu_\delta) = (-5.9 \pm 11.8, 6.0 \pm 20.3) \text{ mas yr}^{-1}$. Combining the results gives a measurement of $(\mu_\alpha, \mu_\delta) = (-11 \pm 9, -1 \pm 15) \text{ mas yr}^{-1}$, consistent with a nondetection. Note that correction to the local standard of rest (LSR) for the pulsar involves adjustments at the level of 1 mas yr^{-1} . Since these are much lower than the uncertainties, we ignore these corrections for B1757–24.

We note that our results and those of Thorsett et al. (2002) are not independent, since two epochs of data are common between the two analyses, although the Pie Town link data were not used in the present work. The measurement of Blazek et al. (2006) is completely independent, since they observe the nebula and not the pulsar. However, only one dimension of motion was probed by these authors. We derive a 68% confidence upper limit on the *westward* motion of the pulsar, $\mu_\alpha > -14.9 \text{ mas yr}^{-1}$ ($\mu_\alpha > -24.8 \text{ mas yr}^{-1}$ at 95% confidence), which corresponds to a westward transverse velocity $v_\perp < 360d_5 \text{ km s}^{-1}$ ($v_\perp < 600d_5 \text{ km s}^{-1}$ at 95% confidence). The implications are discussed further below, but we note that such velocity limits are consistent with the velocity distribution of ordinary young radio pulsars (Arzoumanian et al. 2002; Hobbs et al. 2005).

3. PSR B1951+32: OBSERVATIONS AND RESULTS

PSR B1951+32, a 39.5 ms pulsar with $\tau_c = 107 \text{ kyr}$ and a spin-down energy-loss rate $\dot{E} = 10^{36.6} \text{ erg s}^{-1}$, lies near the southwestern edge of the approximately circu-

⁵ All uncertainties are 68% confidence intervals, except where both 68% and 95% intervals are explicitly reported.

⁶ See <http://www.aips.nrao.edu/>

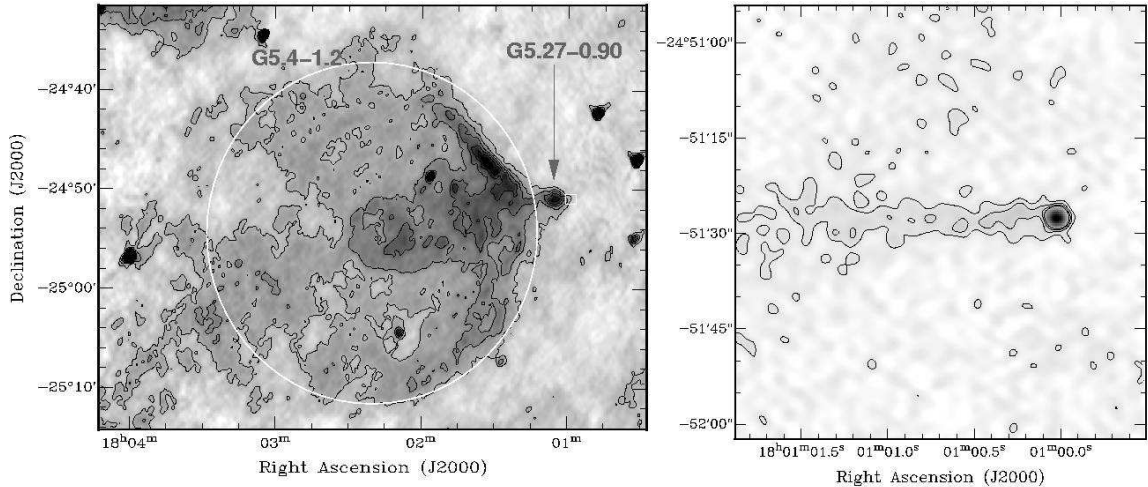


FIG. 1.— The Duck: the SNR G5.4–1.2, G5.27–0.90, and B1757–24 system. *Left*: Large-scale structure of the remnant, as observed by the VLA at 327 MHz with an angular resolution of $40'' \times 23''$ (Brogan et al. 2006, image data courtesy of the authors). The extended circular structure is SNR G5.4–1.2, while G5.27–0.90 is the “head” of the Duck protruding from the west edge of the remnant. The small white square shows the approximate location of the right-hand panel. *Right*: Pulsar B1757–24 and its PWN (the western tip of G5.27–0.90), as observed at 1.4 GHz in 2002. The large-scale structures are resolved out by the interferometer response, leaving only the “beak” visible at an angular resolution of $2''.2 \times 1''.2$.

TABLE 1
OBSERVATIONAL PARAMETERS FOR B1757–24

Epoch	Obs. Code	Poln.	Gated	Flux density (mJy)	rms noise (mJy beam ⁻¹)	Beam (")	Pos. angle	T _{int} (hr)
1998 Jun 03	AF336	R	Y	5.0	0.3	2.3×1.2	16°	1.7
		L	N	1.9	0.1	2.2×1.2	16°	1.7
2001 Jan 01	AB969	R	Y	3.4	0.2	2.3×1.2	-1°	3.2
		L	N	1.1	0.1	2.2×1.2	0°	3.2
2002 Feb 21	AB1029	R	Y	3.4	0.2	2.0×1.2	5°	1.5
2002 May 02	AB1029	I	N	4.5	0.1	2.2×1.2	4°	2.3
2004 Dec 09	AB1139	I	N	1.3	0.1	2.3×1.2	0°	3.5

NOTE. — All observations are at a frequency of 1.45 GHz. Pulsar gating improves the apparent pulsar flux density by a factor $\lesssim [(T_{\text{on}} + T_{\text{off}})/T_{\text{on}}]^{1/2}$.

TABLE 2
REFERENCE SOURCES USED IN THE PROPER MOTION FIT OF B1757–24

R.A. (J2000)	Decl. (J2000)	Flux density (mJy beam ⁻¹)	θ_{sep} (')
18 01 27.40	-25 07 38.1	8.7(2)	17.3
18 01 58.57	-24 55 48.5	6.6(2)	14.0
18 00 47.31	-24 42 45.0	2.6(1)	9.2
18 00 15.71	-25 00 22.0	3.6(1)	13.4
18 01 28.11	-24 34 23.7	1.2(2)	18.2
18 00 41.14	-24 42 04.4	4.9(1)	10.3

NOTE. — Units of right ascension are hours, minutes, and seconds, and units of declination are degrees, arcminutes, and arcseconds.

lar infrared shell of CTB 80 (Fesen et al. 1988). The pulsar is surrounded by a $\sim 30''$ diameter asymmetric PWN at the western edge of an $8' \times 4'$ east-west plateau of emission (Castelletti et al. 2003). CTB 80, observed at 1.4 GHz to have three arms that cover 1.8 deg^2 and converge near B1951+32 (Castelletti et al. 2003), has an expanding H I shell that yields a dynamical age estimate of 77 kyr for the pulsar-SNR system (Koo et al. 1990). From its dispersion measure, the distance to B1951+32 is estimated as $3.1 \pm 0.2 \text{ kpc}$ (Cordes & Lazio 2002), while

the distance to CTB 80 is estimated as 2 kpc from H I absorption (Strom & Stappers 2000). Here we adopt a distance of $2d_2 \text{ kpc}$. Kulkarni et al. (1988) estimated a speed of 300 km s^{-1} for the pulsar from scintillation measurements, while Migliazzo et al. (2002) directly measure a proper motion $\mu = 25 \pm 4 \text{ mas yr}^{-1}$ at a position angle $252^\circ \pm 7^\circ$ after correcting for the effects of differential Galactic rotation. Their implied transverse velocity of the pulsar is $V_{\perp} = (240 \pm 40) d_2 \text{ km s}^{-1}$.

In the direction of the proper motion vector measured by Migliazzo et al. (2002), Moon et al. (2004) observe a cometary X-ray synchrotron nebula and an H α bow shock. The X-ray emission peaks at the pulsar location and is confined within the H α structure (Hester 2000) that is clearly defined at an angular separation of $\sim 7''$ from the pulsar. The X-rays are produced by synchrotron emission from the pulsar wind, confined within a bow shock produced by the ram pressure of the wind interacting with the SNR wall.

In radio images, B1951+32 appears to be situated just inside a limb-brightened bubble $\sim 30''$ in diameter (see Fig. 2, *right*). A $5''$ portion of the bubble nearest to the pulsar is substantially brighter than any other portion of the shell. In MERLIN observations at 1.6 GHz with $0.15''$ resolution, Golden et al. (2005) find that the radio-bright arc shows compact structure, resembling a radio

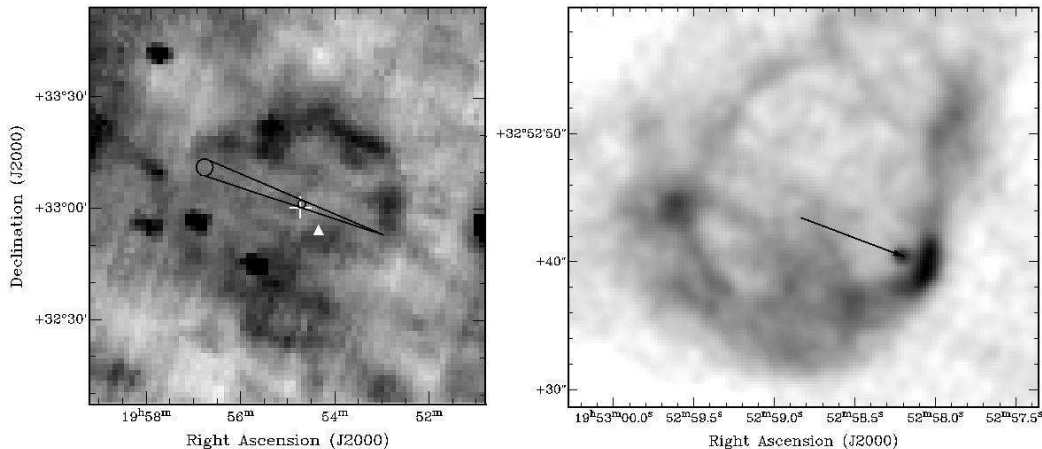


FIG. 2.— CTB 80 (G69.0+2.7) and the PWN produced by PSR B1951+32. *Left:* Infrared ratio image ($60\mu\text{m}/100\mu\text{m}$) constructed from the *IRAS* archive shows the nearly complete shell of CTB 80. Overplotted lines indicate the projected path of the pulsar, projected back in time with the 1σ uncertainty on the measured proper motion, corrected to the LSR. Circles indicate the estimated birth locations for age estimates of $\tau_p \sim 51$ kyr (the age of closest approach to the SNR geometric center, as shown with the white cross) and the characteristic (spin-down) age $\tau_c = 107$ kyr. The projected path does not pass close to the expansion center obtained by Koo et al. (1990), indicated by the white triangle. *Right:* VLA 1.4 GHz image of B1951+32 and its PWN, with an angular resolution of $1''.0 \times 0''.9$ and rms noise 0.03 mJy beam $^{-1}$. The arrow represents 300 yr of travel along the proper motion vector (see §3.2). The bow shock is visible as the bright arc to the south-west of the pulsar. Note the difference in scale between the two panels.

bow shock. The structure is $\sim 2.5''$ from the pulsar, which puts it at the head of the cometary X-ray nebula, but enclosed within the $\text{H}\alpha$ bow shock which is $\sim 7''$ away from the pulsar (Moon et al. 2004).

3.1. Observations

Measurements of the proper motion of PSR B1951+32 were made using five epochs of archival VLA data from 1989.04 to 2003.50. Observation details are shown in Table 3. All observations were made with the VLA A array except the 2000 November 25 epoch, which included the Pie Town antenna. To maintain consistent u - v coverage in each epoch, the baselines to Pie Town were removed before data were reduced. Observations were made with 15 channels of 1.56 MHz each. Data were calibrated with VLA calibrator sources 3C 286 (for flux density and bandpass calibration) and J1925+211 (for phase calibration), following the method outlined in §2.1. Nineteen sources with compact structure were found in the field of view and were included in the imaging and self-calibration process. Eight pointlike sources (see Table 4) were used in the determination of the proper motion in the manner described in §2.1.

The pulsar B1951+32 lies in a complicated region of the CTB 80 SNR and is embedded in its PWN, making the position fit sensitive to observation parameters such as observing frequency and u - v coverage at each epoch. To account for this to first order, a linear brightness gradient in a $1.75''$ square around the pulsar was fit simultaneously with the pulsar position. Trial fits performed without this procedure resulted in substantially greater scatter in the position measurements. Additional trials demonstrated that the fit was not very sensitive to the exact size and position of the region fitted.

3.2. Results

The proper motion of B1951+32 was measured as $(\mu_\alpha, \mu_\delta) = (-28.8 \pm 0.9, -14.7 \pm 0.9)$ mas yr $^{-1}$. Figure 3 demonstrates the significance of the proper motion relative to that of the eight presumably stationary sources

used to define the frame in which the proper motion was measured. For each of the reference sources, we derive a proper motion in the frame defined by the seven other sources. As shown in Figure 3, these proper motion values are consistent with zero at $\sim 1\sigma$, indicating that a self-consistent reference frame has been established.

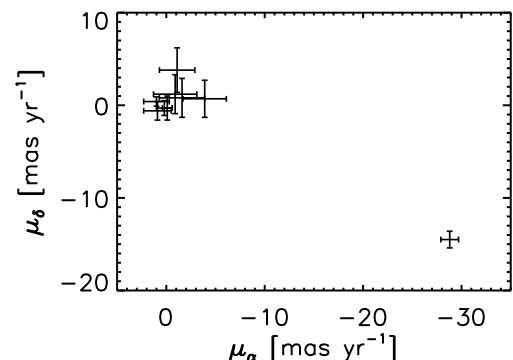


FIG. 3.— Proper motion of PSR B1951+32 and the reference sources used for the fit. Reference source motions with respect to each other are consistent with noise with and scattered around zero. The pulsar lies in the bottom right corner with a proper motion of $(\mu_\alpha, \mu_\delta) = (-28.8 \pm 0.9, -14.7 \pm 0.9)$ mas yr $^{-1}$. In this figure the derived motion of the pulsar is relative to the frame defined by all eight reference sources.

A significant correction is required to obtain the motion of the pulsar in its LSR so that it can be related to the remnant. We use a flat Galactic rotation curve with velocity 220 km s $^{-1}$ and assume a solar radius of 8.5 kpc. Further correction for the solar peculiar motion is applied (Dehnen & Binney 1998). The magnitude of the correction depends on the distance; an additional 0.6 mas yr $^{-1}$ has been added in quadrature to the proper motion uncertainty to accommodate the magnitude range of the correction over the 1 – 3 kpc distance range considered. The LSR-corrected proper motion is found to be $(\mu'_\alpha, \mu'_\delta) = (-26.9 \pm 1.1, -10.5 \pm 1.1)$ mas yr $^{-1}$, for a total proper motion $\mu' = 29 \pm 1$ mas yr $^{-1}$ at a position angle

TABLE 3
OBSERVATIONAL PARAMETERS FOR B1951+32

Epoch	Obs. Code	IF	Pol.	Freq. (MHz)	Flux density (mJy)	rms noise (mJy beam ⁻¹)	Beam (")	Position Angle (")	T _{int} (hr)
1989 Jan 13	AS357	1	RR	1385	1.01	0.07	1.1×1.1	50°	5.9
			LL	1652	0.62	0.09	1.0×0.9	81°	5.9
1991 Jul 18	AF214	1	RR	1385	1.95	0.08	1.3×1.2	-47°	5.8
			LL	1652	1.32	0.08	1.0×0.9	-74°	5.8
1993 Jan 08	AF235	1	RR	1385	1.75	0.06	1.2×1.2	-64°	5.9
			LL	1652	1.79	0.05	1.1×1.0	-58°	5.9
2000 Nov 25	AG602	1	RR,LL	1385	0.63	0.05	1.3×1.2	-69°	5.2
			RR,LL	1516	0.91	0.07	1.1×1.0	-75°	5.2
2003 Jun 03	AG650	1	RR,LL	1665	1.05	0.03	1.0×0.9	-70°	6.2

TABLE 4
REFERENCE SOURCES USED IN THE PROPER MOTION FIT OF B1951+32

R.A. (J2000)	Decl. (J2000)	Flux density (mJy beam ⁻¹)	θ _{sep} (')
19 53 23.70	+32 53 35.3	4.7(3)	5.4
19 53 16.37	+32 48 46.5	21.7(3)	5.5
19 53 17.92	+32 49 11.4	6.8(3)	5.4
19 53 13.42	+33 01 21.8	97.8(3)	9.3
19 52 45.25	+33 03 30.0	6.2(3)	11.2
19 52 15.80	+32 49 35.7	839.3(8)	9.4
19 52 30.01	+32 55 26.2	5.4(3)	6.5
19 52 13.32	+32 59 22.1	61.7(3)	11.6

NOTE. — Units of right ascension are hours, minutes, and seconds, and units of declination are degrees, arcminutes, and arcseconds.

249 ± 2° east of north.

3.3. Shock Separation

To maximize sensitivity to the extended structure of the shock, all u - v data within each epoch were added with the AIPS task DBCON. Before reimagining, the resulting data were convolved with a circular beam with a 1.2'' diameter, the longest semi-major axis of any beam in any of the concatenated data sets, to ensure equal sensitivity to large-scale structure across all epochs.

Full hydrodynamical modeling of the shock is beyond the scope of the present work. Instead, we simply extract the flux density in slices along the observed proper motion vector in the LSR (position angle = 249° east of north) in order to estimate the angular separation between the pulsar and the shock structure at each epoch. As shown in Figure 4, the pulsar position is well defined in these slices, but the transverse structure of the shock changes with epoch and the separation of the pulsar from the shock peak ($\Delta\theta_{\text{Peak}}$) varies between 2.4'' and 3.1''. At each epoch, given the map rms noise σ , we define the shock thickness as the range where the emission is within 1 σ of the shock peak. The near and far edges of the shock, defined in this manner, are listed in Table 5 and indicated in Figure 4.

Over the 14.5 yr span of observations, the pulsar moves by $\sim 0.47''$, but the distance between the pulsar and the near edge of the shock is $\sim 2.1'' \pm 0.2''$ and the separation to the far edge is $\sim 3.6'' \pm 0.6''$. Since the separation between the pulsar and the radio-bright feature does not show a secular decreasing trend, we concur with previous inferences (Hester & Kulkarni 1988; Chatterjee & Cordes 2002) that the feature must be a shock driven by the pulsar wind as the pulsar travels

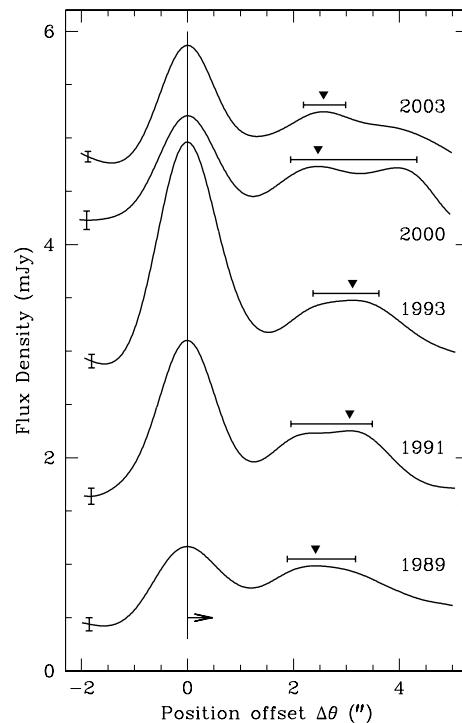


FIG. 4.— Slices through PSR B1951+32 and its bow shock. The flux density is plotted as a function of the offset from the derived pulsar position (as indicated by the solid line), along the measured proper motion vector. Successive epochs are vertically displaced by 1 mJy (except for 2003, which is displaced by 1.25 mJy) for clarity, but note that the time interval between successive observations is not uniform. The map rms noise σ at each epoch is indicated by the error bar at the far left. The peak of the shock is marked, and the width of the shock within 1 σ of the shock peak is also shown by the horizontal error bar. The measured separation is consistent with being constant over ~ 14.4 yr, while the pulsar moves $\sim 0.47''$ in that time period, as shown by the horizontal arrow.

through the ambient medium.

4. DISCUSSION

4.1. The Association between SNR G5.4–1.2 and PSR B1757–24

The identity of the remnant associated by birth with the pulsar B1757–24 is still a mystery. Based on morphology and location, SNR G5.4–1.2 is the only known remnant likely to be related to the pulsar, but that association has serious problems (see Blazek et al. [2006] for a recent discussion). To remain tenable, such an association requires a pulsar age much larger than the character-

TABLE 5
ANGULAR SEPARATION BETWEEN
PSR B1951+32 AND THE RADIO
BOW SHOCK

Epoch	$\Delta\theta_{\text{Peak}}$ ($''$)	$\Delta\theta_{\text{Near}}$ ($''$)	$\Delta\theta_{\text{Far}}$ ($''$)
1989	2.4	1.9	3.2
1991	3.1	2.0	3.5
1993	3.1	2.4	3.6
2000	2.5	1.9	4.3
2003	2.6	2.2	3.0

NOTE. — We list the angular distance from the pulsar peak to the peak of the shock and the range within 1σ of the shock peak at each epoch. The position fit uncertainties are insignificant compared to the thickness of the shock itself.

istic age $\tau_c = 15.5$ kyr, an explosion site much closer to the current location of the pulsar, or some combination of the two. For example, G5.4–1.2 could be expanding into a region with a density gradient (e.g., Gvaramadze 2004). The brightening of the remnant on the western limb, the side nearer to the Galactic plane, may be evidence for such an asymmetric expansion. However, even in an optimistic scenario, the birth site could be no closer than the westernmost limb of G5.4–1.2. In such a case, for a true age $\leq \tau_c$, a westward proper motion $\gtrsim 18$ mas yr $^{-1}$ is required for an association, but all three measurements reported in Table 6, where we summarize our results, imply westward motions no greater than 15 mas yr $^{-1}$. It thus appears that either the true age is larger than τ_c , probably significantly so, or the association of the pulsar with G5.4–1.2 must be excluded.

We note that the characteristic ages of some young pulsars with well-determined kinetic ages are overestimates, for example, J1811–1925 (Kaspi et al. 2001b), J0538+2817 (Ng et al. 2007), and B1951+32 (Migliazzo et al. 2002, our §4.2). Thus, the true age of B1757–24 might be no greater than 15.5 kyr, rendering the association unlikely. But Vela, for example, may have a true age greater than τ_c (Lyne et al. 1996), and Blazek et al. (2006) argue that a growing surface magnetic field, which decouples the true age from the characteristic age, could account for such an age discrepancy in the Duck while preserving the association. Given a long enough time baseline, the pulsar proper motion (or the motion of the nebula) will surely be detectable, allowing a firm conclusion about this vexing association.

4.2. The Age and Bow Shock of B1951+32

For B1951+32, we measure a proper motion of $(\mu_\alpha, \mu_\delta) = (-28.8 \pm 0.9, -14.7 \pm 0.9)$ mas yr $^{-1}$, confirming and improving on the results of Migliazzo et al. (2002). Migliazzo et al. (2002) filter the u - v plane to remove all spatial scales greater than $4''$ and to leave only compact sources. We use a different approach to remove the complexity of the PWN, subtracting the linear slope of the PWN from the region around the pulsar in the image domain. The inclusion of a longer time baseline and a larger field of reference sources increases both the precision and the accuracy of this measurement over that of Migliazzo et al. (2002). The new measurement

corresponds to an LSR-corrected transverse velocity of (274 ± 12) d_2 km s $^{-1}$. At a position angle of 249° , the proper motion vector is well matched to the long symmetry axis of the X-ray PWN (Moon et al. 2004).

The measurement of the proper motion allows a revised estimate for the age of the pulsar. The LSR-corrected proper motion of the pulsar is shown in Figure 2. In projection, its closest approach to the expansion center estimated by Koo et al. (1990) is $\sim 330''$, a 5.5σ deviation assuming a $1'$ uncertainty in the reported expansion center. A geometric center at coordinates 19h54m50s, $33^\circ 00' 30''$ (J2000.0) was estimated by superposing a circle on the remnant shell seen in the left panel of Figure 2. The pulsar’s closest approach to this point implies an age $t_p \sim 51$ kyr with a minimum separation of $74''$, consistent with the $56''$ positional uncertainty based solely on the proper motion uncertainty. Our measurement of the pulsar motion is therefore not consistent with the ~ 77 kyr age and the expansion center estimated by Koo et al. (1990) for the CTB 80 SNR, but it is consistent with the pulsar age determined by Migliazzo et al. (2002). We note that the true explosion center may be masked by asymmetric expansion due, for example, to density gradients and structure in the ISM, and neither estimate for the age may be correct. However, the true age is almost certainly less than $\tau_c \sim 107$ kyr, since the pulsar reaches the far edge of the SNR when its measured proper motion is projected backwards over that time interval, as shown in Figure 2.

As B1951+32 moves through its ambient medium, its relativistic wind outflow is confined by ram pressure, and as seen in some other PWNe, synchrotron emission from the confined pulsar wind produces a cometary X-ray nebula. On the other side of the contact discontinuity, the shocked ISM produces H α emission (see, e.g., the illustration by Gaensler et al. 2004). In such a picture, the radio-bright arc would be produced by the confined pulsar wind at the location of the contact discontinuity. As we have shown here, the structure of the bright arc is dynamic, changing from epoch to epoch, but overall, it moves with the pulsar at an approximately steady separation $\sim 2.5''$, corresponding to a standoff distance of $\sim 0.024 d_2$ pc.

4.3. Two Similar Pulsars in Very Different Environments

Currently, over 1600 radio pulsars have measured values for P and \dot{P} , as listed in the ATNF pulsar catalog⁷ (Manchester et al. 2005). In this large ensemble, B1757–24 and B1951+32 are among the fifty most energetic pulsars, with $\dot{E} = 10^{36.4}$ and $10^{36.6}$ erg s $^{-1}$, respectively. They are also among the hundred youngest known pulsars, with characteristic ages $\tau_c = 15.5$ and 107 kyr, respectively. On one hand, the characteristic age of B1951+32 is likely to be an overestimate, since its current spin period is not much greater than the typical birth spin periods of pulsars (Faucher-Giguère & Kaspi 2006), and its kinematic age $t_p \sim 51$ kyr, assuming birth near the center of CTB 80. On the other hand, the upper limits on its westward proper motion suggest that B1757–24 may be substantially older than its characteristic age. Although the true ages of the pulsars differ in

⁷ See <http://www.atnf.csiro.au/research/pulsar/psrcat>

TABLE 6
SUMMARY OF PROPER MOTION MEASUREMENTS

	B1757–24		Ref. 2	B1951+32	
	This work	Ref. 1		This work	Ref. 3
Target	B1757–24	B1757–24	G5.27–0.9	B1951+32	B1951+32
μ_α (mas yr ⁻¹)	-11 ± 9	-2.1 ± 7.0	> -7.9	-28.8 ± 0.9	-29 ± 2
μ_δ (mas yr ⁻¹)	-1 ± 15	-14 ± 13	...	-14.7 ± 0.9	-8.7 ± 1.3
Time Baseline (yr)	6.5	3.9	12.0	14.5	11.9
Frequency (GHz)	1.4	1.4	8.5	1.4	1.4
RA of Pulsar	18 01 00.016±0.008			19 52 58.206±0.001	
DEC of Pulsar	-24 51 27.5±0.2			32 52 40.51±0.01	
Epoch of RA, DEC	2004 Dec 09			2003 Jun 03	

REFERENCES. — (1) Thorsett et al. (2002); (2) Blazek et al. (2006); (3) Migliazzo et al. (2002)

NOTE. — All provided uncertainties and limits are 68% confidence intervals. Blazek et al. (2006) do not measure μ_δ , and their 68% μ_α has been inferred from their 5 σ limit; results of Migliazzo et al. (2002) have been adjusted to remove the differential Galactic rotation applied in the published result. Proper motions and positions are reported in J2000.0 coordinates and do not include LSR corrections. Units of right ascension are hours, minutes, and seconds, and units of declination are degrees, arcminutes, and arcseconds.

relation to their respective characteristic ages, these two pulsars are quite similar in energetics and age.

Both pulsars also exhibit cometary PWNe. B1757–24 is associated with a $\sim 10''$ elongated nebula visible at both radio (as in Fig. 1) and X-ray wavelengths (Kaspi et al. 2001a). B1951+32 shows a cometary PWN in X-rays (Moon et al. 2004), but its radio structure resembles a bow shock and an extended, limb-brightened bubble, and it is enclosed by a complex nebula visible in H α (Hester 2000), with extended lobes and a bow shock structure. Hester & Kulkarni (1988) suggest that the pulsar is interacting with the wall of its evolved SNR, and we find that the radio shock structure changes with time while moving with the pulsar. On the other hand, B1757–24 appears to be outside any parent remnant. If indeed it is associated with G5.4–1.2, it would have interacted with the wall of the remnant in the past (as B1951+32 is at present), possibly re-energising the shell

and leaving behind the structure we see as the Duck. Alternatively, the parent remnant of B1757–24 is no longer visible, and we are witnesses to a cosmic coincidence.

B.R.Z. acknowledges support from the Research Experiences for Undergraduates program of the National Science Foundation and the Department of Scientific and Academic Affairs of the National Radio Astronomy Observatory (NRAO) for funding this research. S.C. acknowledges support from the University of Sydney Postdoctoral Fellowship program, and he was previously a Jansky Fellow of the NRAO. The VLA is a facility of the NRAO, funded by the NSF and operated under cooperative agreement by Associated Universities, Inc. We thank Dale Frail for helpful conversations regarding this research, and Crystal Brogan for providing the 327 MHz image of G5.4–1.2. *Facilities:* VLA

REFERENCES

- Arzoumanian, Z., Chernoff, D. F., & Cordes, J. M. 2002, *ApJ*, 568, 289
- Blazek, J. A., Gaensler, B. M., Chatterjee, S., van der Swaluw, E., Camilo, F., & Stappers, B. W. 2006, *ApJ*, 652, 1523
- Brogan, C. L., Gelfand, J. D., Gaensler, B. M., Kassim, N. E., & Lazio, T. J. W. 2006, *ApJ*, 639, L25
- Castelletti, G., Dubner, G., Golap, K., Goss, W. M., Velázquez, P. F., Holdaway, M., & Rao, A. P. 2003, *AJ*, 126, 2114
- Chatterjee, S., & Cordes, J. M. 2002, *ApJ*, 575, 407
- Cordes, J. M., & Lazio, T. J. W. 2002, *ArXiv e-print*, astro-ph/0207156
- Dehnen, W., & Binney, J. 1998, *MNRAS*, 294, 429
- Faucher-Giguère, C.-A. & Kaspi, V. M. 2006, *ApJ*, 643 332
- Fesen, R. A., Saken, J. M., & Shull, J. M. 1988, *Nature*, 334, 229
- Frail, D. A., Kassim, N. E., & Weiler, K. W. 1994, *AJ*, 107, 1120
- Frail, D. A., & Kulkarni, S. R. 1991, *Nature*, 352, 785
- Gaensler, B. M., & Frail, D. A. 2000, *Nature*, 406, 158
- Gaensler, B. M., van der Swaluw, E., Camilo, F., Kaspi, V. M., Baganoff, F. K., Yusef-Zadeh, F., & Manchester, R. N. 2004, *ApJ*, 616, 383
- Golden, A., Bourke, S., Clyne, G., Butler, R. F., Shearer, A., Muxlow, T. W. B., & Briskin, W. F. 2005, *ApJ*, 635, L153
- Gvaramadze, V. V. 2004, *A&A*, 415, 1073
- Hester, J. J., & Kulkarni, S. R. 1988, *ApJ*, 331, L121
- Hester, J. 2000, *BAAS*, 32, 1542
- Hobbs, G., Lorimer, D. R., Lyne, A. G., & Kramer, M. 2005, *MNRAS*, 360, 974
- Kaplan, D. L., Frail, D. A., Gaensler, B. M., Gotthelf, E. V., Kulkarni, S. R., Slane, P. O., & Nechita, A. 2004, *ApJS*, 153, 269
- Kaplan, D. L., Gaensler, B. M., Kulkarni, S. R., & Slane, P. O. 2006, *ApJS*, 163, 344
- Kaspi, V. M., Gotthelf, E. V., Gaensler, B. M., & Lyutikov 2001a, *M. ApJ*, 562, L163
- Kaspi, V. M., Roberts, M. E., Vasisht, G., Gotthelf, E. V., Pivovarov, M., & Kawai, N. 2001b, *ApJ*, 560, 371
- Koo, B.-C., Reach, W. T., Heiles, C., Fesen, R. A., & Shull, J. M. 1990, *ApJ*, 364, 178
- Kulkarni, S. R., Clifton, T. C., Backer, D. C., Foster, R. S., & Fruchter, A. S. 1988, *Nature*, 331, 50
- Lyne, A. G., Pritchard, R. S., Graham-Smith, F., & Camilo, F. 1996, *Nature*, 381, 497
- Manchester, R. N., Hobbs, G. B., Teoh, A. & Hobbs, M., 2005, *AJ*, 129, 1993
- Manchester, R. N., Kaspi, V. M., Johnston, S., Lyne, A. G., & D’Amico, N. 1991, *MNRAS*, 253, 7P
- McGary, R. S., Briskin, W. F., Fruchter, A. S., Goss, W. M., & Thorsett, S. E. 2001, *AJ*, 121, 1192
- Migliazzo, J. M., Gaensler, B. M., Backer, D. C., Stappers, B. W., van der Swaluw, E., & Strom, R. G. 2002, *ApJ*, 567, L141

- Moon, D.-S., Lee, J.-J., Eikenberry, S. S., Koo, B.-C., Chatterjee, S., Kaplan, D. L., Hester, J. J., Cordes, J. M., Gallant, Y. A., & Koch-Miramond, L. 2004, *ApJ*, 610, L33
- Ng, C.-Y., Romani, R. W., Bricken, W. F., Chatterjee, S., & Kramer, M. 2007, *ApJ*, 654, 487
- Seward, F. D., Slane, P. O., Smith, R. K. & Sun, M. 2003, *ApJ*, 584, 414
- Strom, R. G., & Stappers, B. W. 2000, in *ASP Conf. Ser. 202: IAU Colloq. 177: Pulsar Astronomy - 2000 and Beyond*, ed. M. Kramer, N. Wex, & R. Wielebinski, 509
- Thorsett, S. E., Bricken, W. F., & Goss, W. M. 2002, *ApJ*, 573, L111
- Vasisht, G., & Gotthelf, E. V. 1997, *ApJ*, 486, L129